Two-Photon Selective Excitation of Phonon-Mode in Diamond Using Mid-Infrared Free-Electron Laser

Oji Sato[a], Kyohei Yoshida[b], Heishun Zen[c], Kan Hachiya[a,*], Takuya Goto[d], Takashi Sagawa[a], Hideaki Ohgaki[c]

[a] *Graduate School of Energy Science, Kyoto University, Yoshida-honmachi, Sakyo-ku, Kyoto 606-8501, Japan*
[b] *Institute of Chemistry and Biology of Membranes and Nano-objects, University of Bordeaux, 2 Rue Robert Escarpit, 33607 Pessac, France*
[c] *Institute of Advanced Energy, Kyoto University, Gokasho, Uji, Kyoto 611-0011, Japan*
[d] *Graduate School of Science and Engineering, Doshisha University, 1-3 Tatara Miyakodani, Kyotanabe, Kyoto 610-0394, Japan*

Abstract

Two-photon selective excitation of an infrared (IR)-inactive phonon mode by a mid-infrared tunable free-electron laser (FEL) was accomplished. The mode-selective phonon excitation of IR-active mode by one-photon excitation using FEL (K. Yoshida, et al., Appl. Phys. Lett. 103, 182103 (2013)) was extended to the IR-inactive mode excitation. The T_{2g} optical phonon mode in single-crystal diamond at $1,332\ \mathrm{cm}^{-1}$ was selected, and the FEL photon energy corresponding to the oscillation wavelength was tuned to the half of the target phonon energy. The successful mode excitation was confirmed by anti-Stokes Raman scattering signal of T_{2g} for the sample at cryogenic temperature, where all other modes were suppressed. The signal was observed at T_{2g} phonon energy with red-shift of the peak to $1,306\ \mathrm{cm}^{-1}$, which was accompanied by surface damage induced by intense laser irradiations.

Keywords: Selective phonon-mode excitation, Free-electron laser, Raman scattering, Two-photon excitation, Diamond

*Corresponding author
Email address: hachiya@energy.kyoto-u.ac.jp (Kan Hachiya)

1. Introduction

Phonon controls not only thermal and structural properties such as lattice vibration or phase transition, but also electronic structures in materials via electron-phonon coupling, such as electron transport in normal conductivity or in superconductivity, magnetic properties [1–6]. On the other hand, important physical properties are often connected to, not all, but particular mode, and end up in structural and electronic transitions [7–11]. To promote these physical properties strongly connected to single mode, or few modes, it is essential to make clear the role of such modes in a crystal. Nevertheless, multiple phonon modes are excited at once through usual thermal phonon excitation, from ground state to upper states at around finite thermal energy corresponding to the absolute temperature, as is enlightened by statistical mechanics. In order to excite the target mode one by one, the coherent phonon spectroscopy technique [12, 13] is the most typical method [14–19]. It has been successfully applied to clarify the relationship between each mode and the emergence of the above physical properties [2, 3, 6–11].

In previous reports, some of the present authors have proposed an alternative method with a simpler and straightforward approach, involving the direct pumping of the phonon energy through the irradiation of mid-infrared (MIR) free-electron-laser (FEL) whose photon energy is equal to that of the target phonon [20, 21]. Selective excitation of the particular phonon in 6H-SiC and GaN were demonstrated. This method is expected to stabilize the excited vibrational state against mode transition [2, 22]. Nevertheless, the selective phonon excitation method in Ref. [20] is a one-photon absorption for the one-phonon excitation, and it was applied only to so-called IR active vibrational modes. This restriction within allowance arising from the one-photon-absorption selection rule principle can be largely bypassed by two-photon absorption. Several approaches have been made for the selective excitation of the IR-inactive mode. Among one of such mode for example, the excitation of an optical phonon of diamond near Γ point ($T_{2g} = F_{2g} = \Gamma_{25'}$) at around $1,332$ cm^{-1} (= 40

THz = 7.5 μm) was demonstrated by the coherent phonon excitation [18, 19] and direct excitation with a pump pulse via difference-frequency mixing of two parametrically amplified pulse trains from a single white-seed whose center frequencies are continuously tunable between $10 - 72$ THz [23]. The T_{2g} optical phonon in boron-doped diamonds is known to be related to superconductivity [24]. With high symmetry of the diamond, high selectivity of the light source for excitation is not absolutely necessary, because the other competing modes are limited and separated from the target mode. Nevertheless, the selectivity is essential in order to establish the method of selective phonon-mode excitation to investigate the phonon-related solid-state properties including superconductivity mechanism, which is expected to be strongly related to electron-phonon coupling. As for the tune to 20 THz, which is half of the T_{2g} phonon frequency (40 THz), the method with FEL in this study can confine pump laser oscillation spectrum within $19.2 - 20.3$ THz, the bandwidth around 1 THz, in contrast to that of several terahertz [23] which would be only adequate for selective excitation of diamond T_{2g} mode. The present approach of confined bandwidth can be applied not only to investigate, but also to control the superconductivity in crystals of complex structures which have a number of phonon modes. The high-T_c cuprate superconductors of complex perovskite-type layered structures have been expected to manipulate the superconductivity optically [25–28].

Additionally, we adopted anti-Stokes Raman scattering (ASRS) for signal measurements instead of real-time optical Kerr effect observations to confirm successful single mode excitation [23], because the need for the femtosecond-scale ultrafast spectroscopy were eliminated.

The T_{2g} phonon mode in diamond is Raman active and IR inactive. The half of its frequency is within the wavenumber range of the oscillating frequency of the FEL we use (Kyoto University Free-Electron Laser: KU-FEL [29]), which is approximately $435 - 2,850$ cm^{-1} ($3.5 - 23$ μm) at present [30].

2. Two-photon mode-selective phonon excitation

The principle of the mode-selective phonon excitation is given in FIG. 1(c) in Ref. [20]. It is selective phonon excitation to a particular target phonon-excited state with photon from MIR laser.

In one-photon mode-selective phonon excitation [20, 21], the excitation part with pump light is one-photon (linear) absorption from the excitation light. The transition rate, $R^{(1)}$, for this process is given as

$$R^{(1)} = \frac{4\pi^2}{nc} \frac{|\mu_{mg}|}{\hbar^2} \rho_f(\omega) \times I, \tag{1}$$

where n is refraction index, c is the speed of light, μ_{mg} is a transition matrix, $\hbar$ is Planck constant, $\rho_f(\omega)$ is a line shape function, and $\hbar\omega$ corresponds to the energy of pump light of intensity I to excite the phonon mode of $\hbar\omega_{mg}$ [31]. Subscript g indexes ground state and m indexes final state. The lineshape function for the one-photon absorption has its peak at $\omega = \omega_{mg}$, the angular frequency of the target phonon. This part of excitation follows selection rules for one-photon absorption which can be known from the calculation of μ_{mg} and determined by crystal symmetry [32].

In the present study, two-photon absorption from the single beam of pump light is used instead. The transition rate, $R^{(2)}$, for this process is given as

$$R^{(2)} = \frac{8\pi^3}{n^2c^2} \left| \sum_m \frac{\mu_{nm}\,\mu_{mg}}{\hbar^2(\omega_{mg} - \omega)} \right|^2 \rho_f(2\omega) \times I^2, \tag{2}$$

where the lineshape function for the two-photon absorption has its peak at $2\omega = \omega_{ng}$, the angular frequency of the target phonon in this case [31]. Subscript m indexes the medium states for this case, while n indexes final state. The selection rule for the two-photon absorption is determined by $\sum_m \mu_{nm}\,\mu_{mg}$ with the help of the multiplication tables of group theory [32].

As noted in the introduction, we used ASRS for confirmation of the target phonon excitation. Therefore, the selection rules for the phonon detection part with probe light is given by those of the Raman scattering [33, 34].

The selection rules for the present case (T_{2g}-mode excitation) for two-photon absorption and Raman scattering are both classified as optically-allowed transition like many other modes of both IR-inactive and Raman-active selectivities at the same time. This is not the case with one-photon absorption and Raman scattering, at least for the all vibrational modes in the crystals of center of symmetry, and many of the modes in other structure-types of crystals.

The transition rate for two-photon absorption shows quadric dependence on the pump-light intensity, while one-photon absorption shows linear dependence.

3. Experimental methods

The experimental setup for the optical irradiation and measurement system is shown in Fig. 1. An MIR-FEL (KU-FEL) was irradiated as a pumping light source to excite the phonon mode, and a probe light source of 532 nm laser, the second-harmonic wave of the amplified Nd:YVO_4 laser (Time-Bandwidth GE-100-VAN), was selected for the probe in the ASRS measurement [20, 35]. The full width at a half maximum (FWHM) of the pulse time duration is 7.5 ps for the probe laser. The durations of macro- and micro- pulses are 2 μs and 0.6 ps (FWHM) at 12 μm, respectively [36, 37]. The pulse time-width of the micropulse of KU-FEL, which is also 0.6 ps in this method [20], is shorter than the reported phonon lifetime of the phonon in diamonds, $\sim 6 - 8$ ps [18, 23]. Therefore, the MIR-FEL irradiation induces mode-selective phonon excitation via a photoexcitation effect. Rough synchronization (tens of nanoseconds scale) between pump and probe lasers was accomplished using a digital delay generator (Stanford Research Systems DG645). Precise synchronization (sub-picosecond scale) of those lasers was accomplished by the timing stabilizer (Time-Bandwidth CLX-1100) with the reference RF signal which was used for accelerate electron beam in KU-FEL. The temporal overlap condition of those lasers was adjusted by the optical delay stage, and the zero-delay condition between the pump and probe lasers was confirmed by the sum-frequency light generated from a ZnS cleartran (Pier Optics) sample which was placed adjacent to a diamond sample.

The (100) face of a single-crystal diamond (Element six 145-500-0253) was used as the target. It was cooled to 7 K in a cryostat (Taiyo Nippon Sanso 1005 337) equipped with a helium compressor (Sumitomo Heavy Industries CKW-21A). As noted in the figure, a KBr window was set to pass both the MIR pump and 532 nm probe laser light, and a fused silica window was mounted to transmit the transmitted and scattered light.

The scattered light was guided through triply stacked notch filters (Thorlabs NF533-17 $\times$2; Opto-line StopLine notch filter NF03-532E-25 $\times$1) in order to eliminate Rayleigh scattering light of the probe laser, and was detected by photon counting with a photo multiplier (Hamamatsu photonics R3896) after dispersion with a spectrometer (Horiba Scientific Triax 190).

The optical process through two-photon excitation in general can be observed only near the focal spot near the incident laser beam [31]. Consequently, the focal spot of the FEL was adjusted to locate on the sample surface as close as possible, where the Raman scattering signal with probe laser was expected to be maximized at the same time. Nevertheless, this geometry may also cause laser-induced damages especially by pumping laser whose pulse energy is set to a few mJ, rather than those by probe laser of ~ 0.1 mJ pulse energy. A field-emission-type SEM (FE-SEM; Hitachi High-Technologies SU6600) was used to take a photographic image of the single-crystal diamond sample irradiated with focused pumping and probe lasers, in order to confirm the fracture surface created by the damage induced by laser irradiations.

4. Results

We preliminary confirmed the Raman signal of the optical phonon mode of the diamond sample. The spectrum was obtained with the second-harmonic wave of the nano-second Nd:YAG laser (Continuum Surelite SLII-10) as a probe. As presented in Fig. 2, the Raman signal was observed at $1,332$ cm^{-1} at room temperature. In order to excite the phonon by two-photon absorption, the FEL wavelength was tuned to 15.0 μm, which corresponds to $1,333$ cm^{-1} in

two-photon scale. The lower panel of Fig. 3 shows the results of the ASRS measurement with and without FEL irradiation, whose spectrum center is estimated to be $1,306$ cm^{-1} by fitting Gaussian lineshape to the observed scattering band. The FEL spectrum is also given in the upper panel of Fig. 3. The sharp dip in the spectrum arises from absorption by CO_2 in ambient air, though it has negligible impact on the phonon dynamics [23]. The light path from the FEL oscillator output to the sample chamber was consequently replaced with nitrogen gas. The FEL macropulse energy was set to 6.5 mJ. The spectrometer slit width was 1.0 mm. The spectra were obtained using the 200-times average of each point. The pulse energy of the Nd:YVO_4 probe laser was 70 μJ. The ASRS band at around $1,306$ cm^{-1}, assigned to the phonon, followed on/off switching of the pump FEL. Figure 4 shows the pump-energy dependence of the peak intensity at $1,306$ cm^{-1} and a fitted quadratic curve. The coefficient of determination, R^2, for the polynomial regression with quadratic model was 0.950, while it was 0.917 for the linear regression. The consistency with quadratic model function confirms two-photon excitation [31]. Figure 5 shows that ASRS peak intensity at $1,306$ cm^{-1} against delay time of probe laser to pump laser. The ASRS signal was observed between $0 - 13$ ps. If we simply subtract the pulse time duration of the probe laser, ~ 5.5 ps of the phonon lifetime is suggested, which matches with previous reports [18, 23].

Although the obtained Raman scattering band covered the expected ASRS peak position corresponding to T_{2g} phonon energy, the peak position of the band estimated from our measurement was red-shifted. It is reported that the damage induced by helium ion beam bombardment causes red-shift of Raman scattering wavenumber for T_{2g} mode in diamond to $1,297.7$ cm^{-1}, against damage depth of ~ 5 μm [38]. This red-shift of around 30 cm^{-1} also reported to be accompanied by FWHM increase from 3 cm^{-1} to 87.8 cm^{-1} [38]. The FWHM of the observed band in Fig. 3, $\sim$ 120 cm^{-1}, contains additional broadening by FWHM of pumping FEL, which is ~ 50 cm^{-1} also presented in Fig. 3.

Presented in Fig. 6 is a scanning electron microscope (SEM) image of a fracture surface taken by FE-SEM for a sample after the irradiations for the

measurement in Fig. 4 of pumping and probe lasers. These fractures were not found on the sample without laser irradiation. Although the kind of the laser-pulse shot which created the fracture in this image cannot be identified, the peak shift was presumably caused by the damage induced by FEL irradiations as discussed in the experimental section. In order to observe the two-photon excitation signal, the FEL light with sub-mJ micropulses of 0.6 ps of duration, which was a few mJ of macropulse, was maximally focused within the order-of-0.01 mm^2 area estimated from SEM image. Therefore, brittle fractures of the diamond surface were brought about.

5. Conclusion

We confirmed the selective T_{2g} phonon excitation by measuring ASRS signal at 7 K. Mid-infrared FEL light was tuned to half of the optical phonon energy near Γ point in single-crystal diamond at (100) face for single-phonon excitation through two-photon excitation with FEL. The estimated phonon lifetime of a few ps was similar to the previous reports. The peak position was red-shifted at the same time, which was induced by FEL irradiations.

Acknowledgments

The authors are grateful to Takeshi Yabutsuka, Shigeomi Takai, Takayuki Yamamoto, Toshiyuki Nohira and Muneyuki Kagaya. This work was supported by JSPS KAKENHI, Grant-in-Aid for Scientific Research (C), Grant Number 18K05295, and the “Joint Usage/Research Program on Zero-Emission Energy Research”, Institute of Advanced Energy, Kyoto University (ZE30A-13 and ZE31A-17).

References

[1] W. S. Warren, H. Rabitz and M. Dahleh, Coherent control of quantum dynamics: the dream is alive, Science 259 (1993) 1581-1589.

[2] M. Först, C. Manzoni, S. Kaiser, Y. Tomioka, Y. Tokura, R. Merlin and A. Cavalleri, Nonlinear phononics as an ultrafast route to lattice control, Nat. Phys. 7 (2011) 854-856 .

[3] M. Rini, R. Tobey, N. Dean, J. Itatani, Y. Tomioka, Y. Tokura, R. W. Schoenlein and A. Cavalleri, Control of the electronic phase of a manganite by mode-selective vibrational excitation, Nature 449 (2007) 72-74.

[4] G.-H. Gweon, T. Sasagawa, S.Y. Zhou, J. Graf, H. Takagi, D.-H. Lee and A. Lanzara, An unusual isotope effect in a high-transition-temperature superconductor, Nature 430 (2004) 187-190.

[5] H. Anzai, M. Arita, H. Namatame, M. Taniguchi, M. Ishikado, K. Fujita, S. Ishida, S. Uchida and A. Ino, A new landscape of multiple dispersion kinks in a high-T_c cuprate superconductor, Sci. Rep. 7 (2017) 4830.

[6] M. Först, R. I. Tobey, S. Wall, H. Bromberger, V. Khanna, A. L. Cavalieri, Y.-D. Chuang, W. S. Lee, R. Moore, W. F. Schlotter, J. J. Turner, O. Krupin, M. Trigo, H. Zheng, J. F. Mitchell, S. S. Dhesi, J. P. Hill and A. Cavalleri, Driving magnetic order in a manganite by ultrafast lattice excitation, Phys. Rev. B 84 (2011) 241104(R).

[7] D. H. Hurley, R. Lewis, O. B. Wright and O. Matsuda, Coherent control of gigahertz surface acoustic and bulk phonons using ultrafast optical pulses, Appl. Phys. Lett. 93 (2008) 113101.

[8] A. Bartels, T. Dekorsy, H. Kurz and K. Köhler, Coherent control of acoustic phonons in semiconductor superlattices, Appl. Phys. Lett. 72 (1998) 2844-2846.

[9] C.-K. Sun, Y.-K. Huang, J.-C. Liang, A. Abare and S. P. DenBaars, Coherent optical control of acoustic phonon oscillations in InGaN/GaN multiple quantum wells, Appl. Phys. Lett. 78 (2001) 1201-1203.

[10] M. Hase, K. Mizoguchi, H. Harima, S. Nakashima, M. Tani, K. Sakai and M. Hangyo, Optical control of coherent optical phonons in bismuth films, Appl. Phys. Lett. 69 (1996) 2474-2476.

[11] Y. Kasai, D. Suzuki, H. Kunugita and K. Ema, Resonantly excited coherent optical phonons in wide-gap semiconductor ZnTe, J. Lumin. 129 (2009) 1820-1823.

[12] W. A. Kutt, W. Albrecht and H. Kurz, Generation of coherent phonons in condensed media, IEEE J. Quantum Electron. 28 (1992) 2434-2444.

[13] R. Merlin, Generating coherent THz phonons with light pulses, Solid State Commun. 102 (1997) 207-220.

[14] D. M. Riffe and A. J. Sabbah, Coherent excitation of the optic phonon in Si: Transiently stimulated Raman scattering with a finite-lifetime electronic excitation, Phys. Rev. B 76 (2007) 085207.

[15] T. E. Stevens, J. Kuhl and R. Merlin, Coherent phonon generation and the two stimulated Raman tensors, Phys. Rev. B 65 (2002) 144304.

[16] L. Dhar, J. A. Rogers and K. A. Nelson, Time-resolved vibrational spectroscopy in the impulsive limit, Chem. Rev. 94 (1994) 157-193.

[17] Y. Yan, E. B. Gamble and K. A. Nelson, Impulsive stimulated scattering: General importance in femtosecond laser pulse interactions with matter, and spectroscopic applications, J. Chem. Phys. 83 (1985) 5391-5399.

[18] K. Ishioka, M. Hase, M. Kitajima and H. Petek, Coherent optical phonons in diamond, Appl. Phys. Lett. 89 (2006) 231916.

[19] H. Sasaki, R. Tanaka, Y. Okano, F. Minami, Y. Kayanuma, Y. Shikano and K. G. Nakamura, Coherent control theory and experiment of optical phonons in diamond, Sci. Rep. 8 (2018) 9609.

[20] K. Yoshida, T. Sonobe, H. Zen, K. Hachiya, K. Okumura, K. Mishima, M. Inukai, H. Negm, K. Torgasin, M. Omer, T. Kii, K. Masuda and H. Ohgaki, Experimental demonstration of mode-selective phonon excitation of 6H-SiC by a mid-infrared laser with anti-Stokes Raman scattering spectroscopy, Appl. Phys.Lett. 103 (2013) 182103.

[21] M. Kagaya, K. Yoshida, H. Zen, K. Hachiya, T. Sagawa and H. Ohgaki, Mode-selective phonon excitation in gallium nitride using mid-infrared free-electron laser, Jpn. J. Appl. Phys. 56 (2017) 022701.

[22] T. P. Martin and L. Genzel, Ionic Raman scattering and ionic frequency mixing, Phys. status solidi 61 (1974) 493-502.

[23] S. Maehrlein, A. Paarmann, M. Wolf and T. Kampfrath, Terahertz sum-frequency excitation of a Raman-active phonon, Phys. Rev. Lett. 119 (2017) 127402.

[24] M. Hoesch, T. Fukuda, J. Mizuki, T. Takenouchi, H. Kawarada, J. P. Sutter, S. Tsutsui, A. Q. R. Baron, M. Nagao and Y. Takano, Phonon softening in superconducting diamond, Phys. Rev. B 75 (2007) 140508.

[25] Y. Okano, H. Katsuki, Y. Nakagawa, H. Takahashi, K. G. Nakamura and K. Ohmori, Optical manipulation of coherent phonons in superconducting $YBa_2Cu_3O_{7-\delta}$ thin films, Faraday Discuss. 153 (2011) 375-382.

[26] D. Fausti, R. I. Tobey, N. Dean, S. Kaiser, A. Dienst, M. C. Hoffmann, S. Pyon, T. Takayama, H. Takagi, A. Cavalleri, Light-induced superconductivity in a stripe-ordered cuprate, Science 331 (2011) 189-191.

[27] W. Hu, S. Kaiser, D. Nicoletti, C. R. Hunt, I. Gierz, M. C. Hoffmann, M. Le Tacon, T. Loew, B. Keimer and A. Cavalleri, Optically enhanced coherent

transport in $YBa_2Cu_3O_{6.5}$ by ultrafast redistribution of interlayer coupling, Nature Mater. 13 (2014) 705-711.

[28] R. Mankowsky, A. Subedi, M. Först, S. O. Mariager, M. Chollet, H. T. Lemke, J. S. Robinson, J. M. Glownia, M. P. Minitti, A. Frano, M. Fechner, N. A. Spaldin, T. Loew, B. Keimer, A. Georges and A. Cavalleri, Nonlinear lattice dynamics as a basis for enhanced superconductivity in $YBa_2Cu_3O_{6.5}$, Nature, 516 (2014) 71-73.

[29] H. Ohgaki, T. Kii, K. Masuda, H. Zen, S. Sasaki, T. Shiiyama, R. Kinjo, K. Yoshikawa and T. Yamazaki, Lasing at 12 μm mid-infrared free-electron laser in Kyoto University, Jpn. J. Appl. Phys. 47 (2008) 8091-8094.

[30] H. Zen, J. Okumura, S. Tagiri, S. Krainara, S. Suphakul, K. Torgasin, T. Kii, K. Masuda and H. Ohgaki, Present status of infrared FEL facility at Kyoto University, Proc. FEL 2017 (2018) 162-165.

[31] R. W. Boyd, Nonlinear Optics, 2nd Ed. (Academic Press, San Diego, 2003) Chapter 12.

[32] C. F. Klingshirn, Semiconductor Optics, 4th Ed. (Springer, Berlin Heidelberg, 2012) Chapter 26.

[33] R. Loudon, The Raman effect in crystals, Adv. Phys. 13 (1964) 423-482.

[34] P. Y. Yu and M. Cardona, Fundamentals of Semiconductors, 4th Ed. (Springer, Berlin Heidelberg, 2010) §7.2.

[35] T. Murata, H. Zen, T. Katsurayama, T. Nogi, S. Suphakul, K. Torgasin, T. Kii, K. Masuda, H. Ohgaki, K. Yoshida and K. Hachiya, Development of phonon dynamics measurement system by MIR-FEL and pico-second laser, Proc. FEL2015 (2015) 615-617.

[36] H. Zen, M. Inukai, K. Okumura, K. Mishima, K. Torgasin, H. Negm, M. Omer, K. Yoshida, R. Kinjo, T. Kii, K. Masuda and H. Ohgaki, Present

status of Kyoto University free electron laser, Proc. FEL2013 (2013) 711-714.

[37] Y. Qin, H. Zen, X. Wang, T. Kii, T. Nakajima and H. Ohgaki, Pulse duration and wavelength stability measurements of a midinfrared free-electron laser, Opt. Lett. 38 (2013) 1068-1070.

[38] J. O. Orwa, K. W. Nugent, D. N. Jamieson and S. Prawer, Raman investigation of damage caused by deep ion implantation in diamond, Phys. Rev. B 62, 5461-5472 (2000).

List of figures

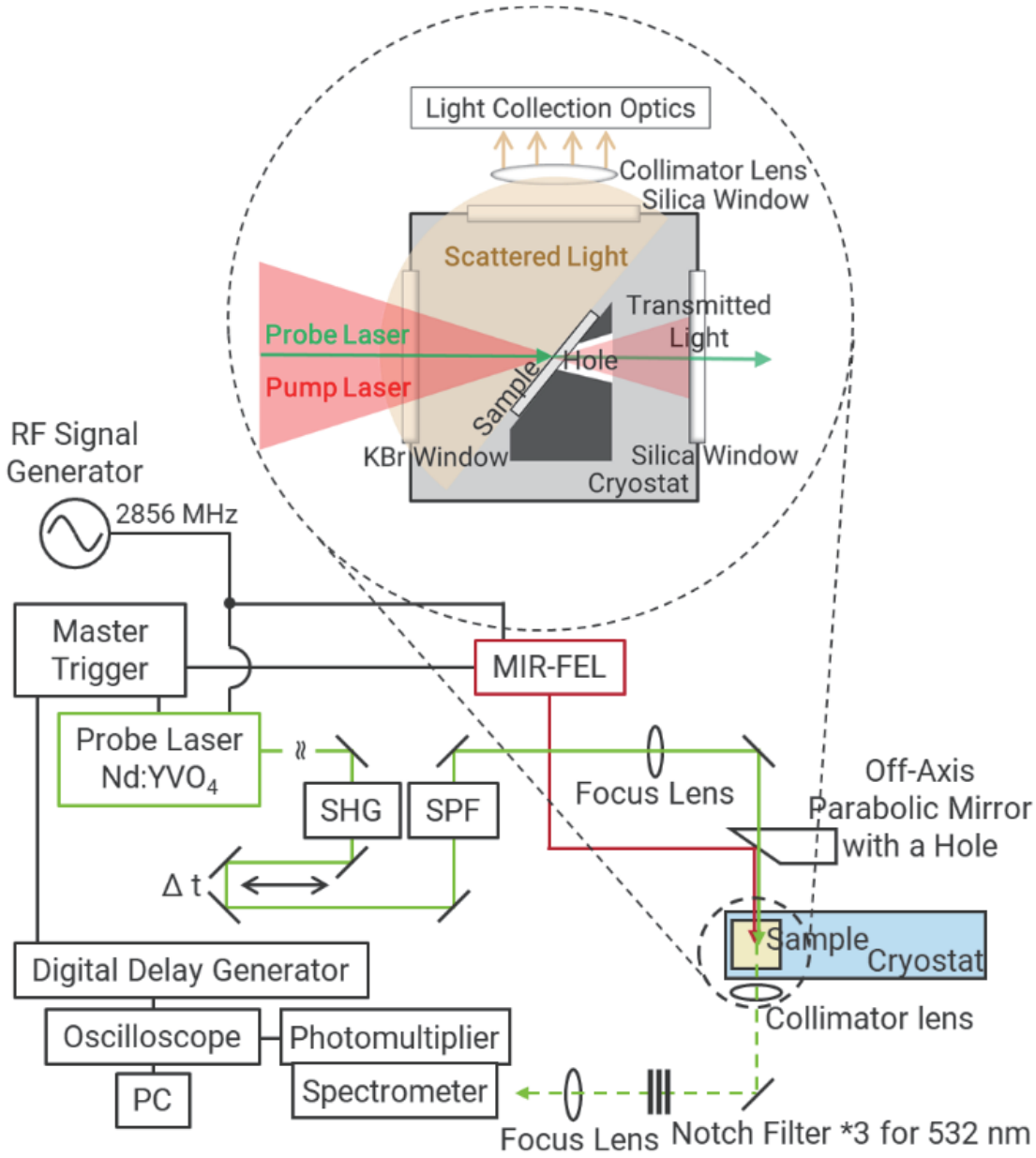

Figure 1: Schematic for the pump MIR-FEL and probe laser irradiations and ASRS measurement (SHG: second-harmonic generation in BBO crystal; SPF: short pass filter cutting off the light longer than 800 nm). The inset shows the geometry around the sample in the cryostat and indicates the spatial configuration of the pump MIR-FEL and probe Nd:YVO_4 laser.

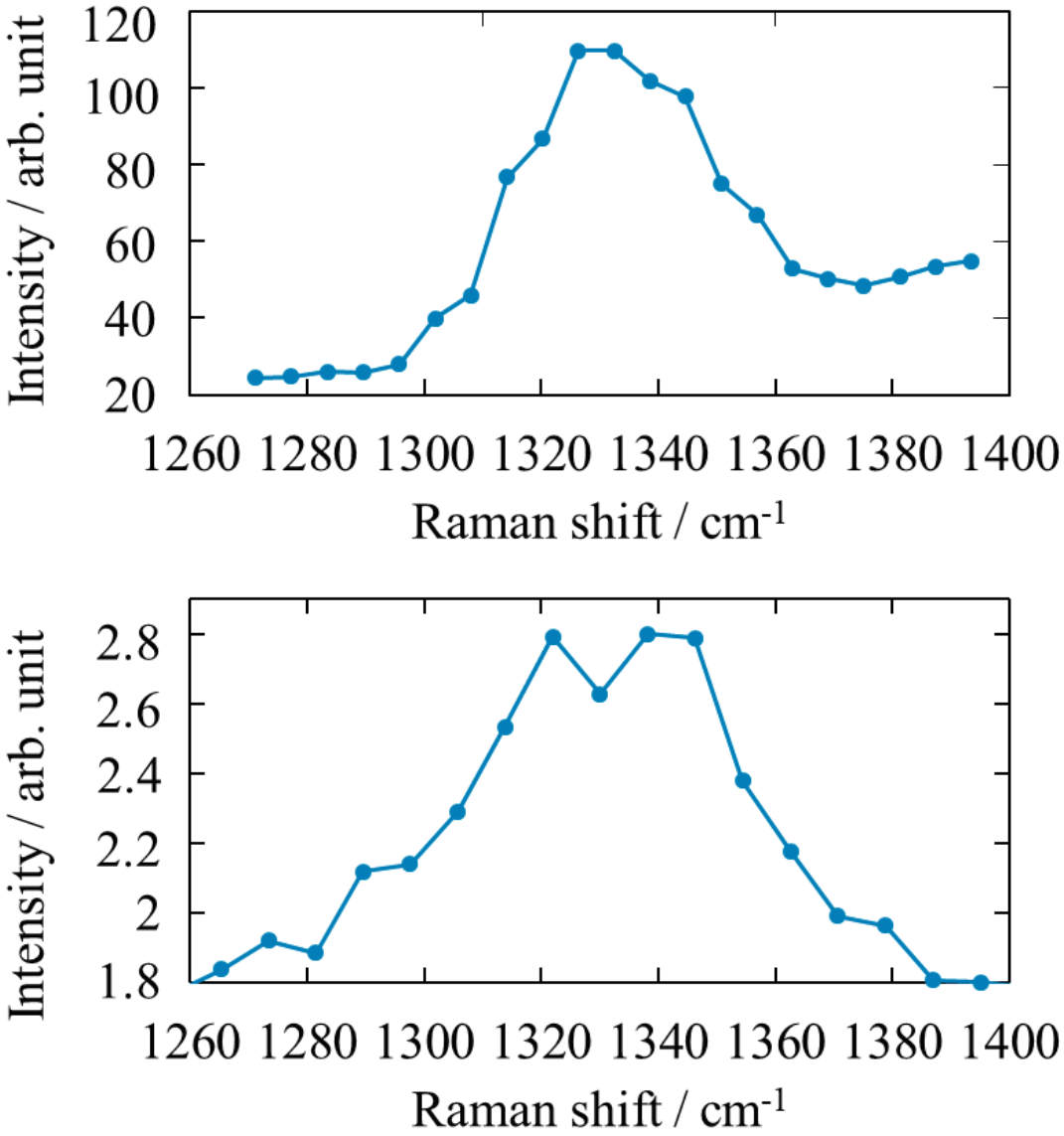

Figure 2: A Stokes (upper panel) and anti-Stokes (lower panel) Raman scattering spectrum of T_{2g} mode of single-crystal diamond (100) face at room temperature.

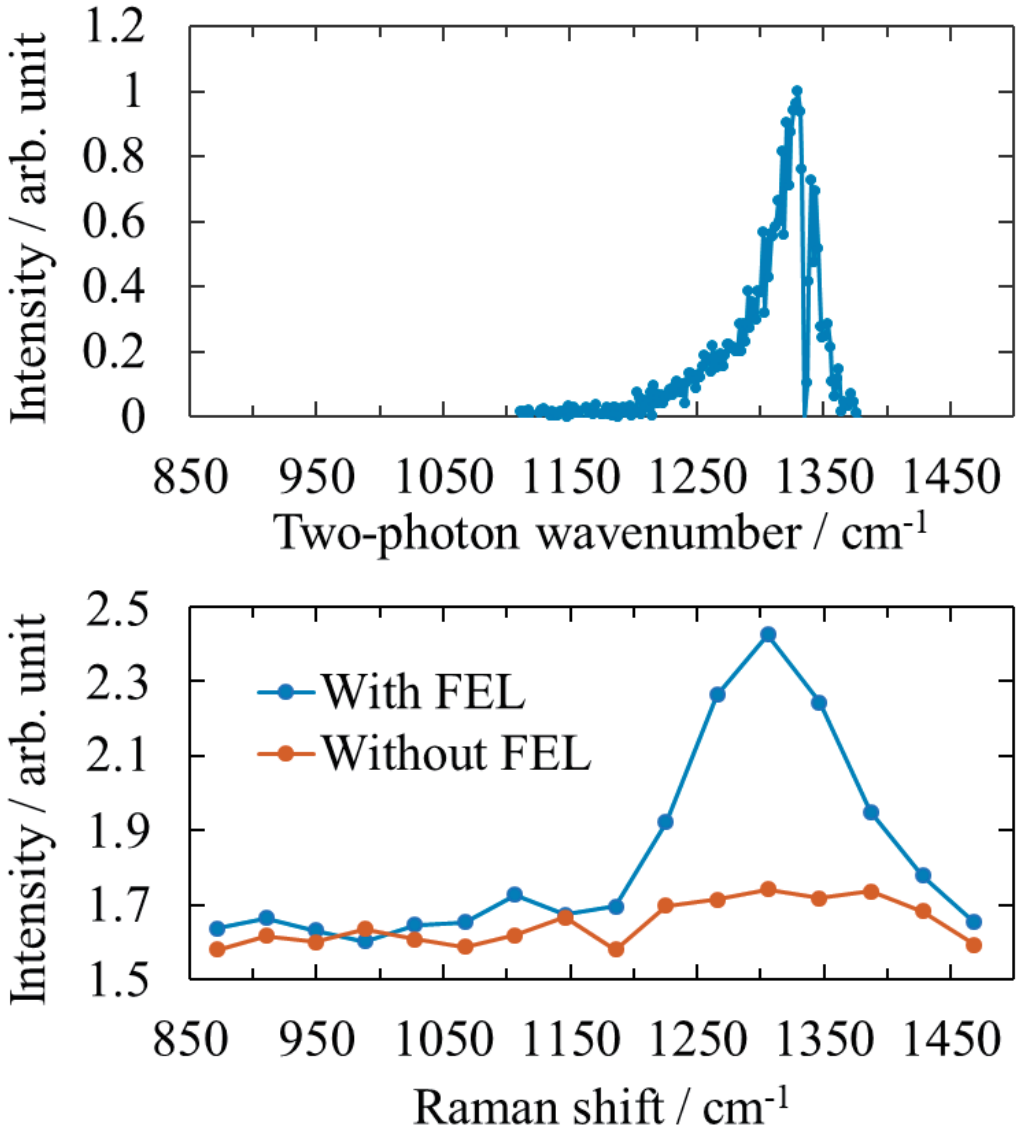

Figure 3: A spectrum of pump FEL light against two-photon wavenumber (upper panel) and spectra obtained by ASRS measurements with and without FEL irradiation (lower panel).

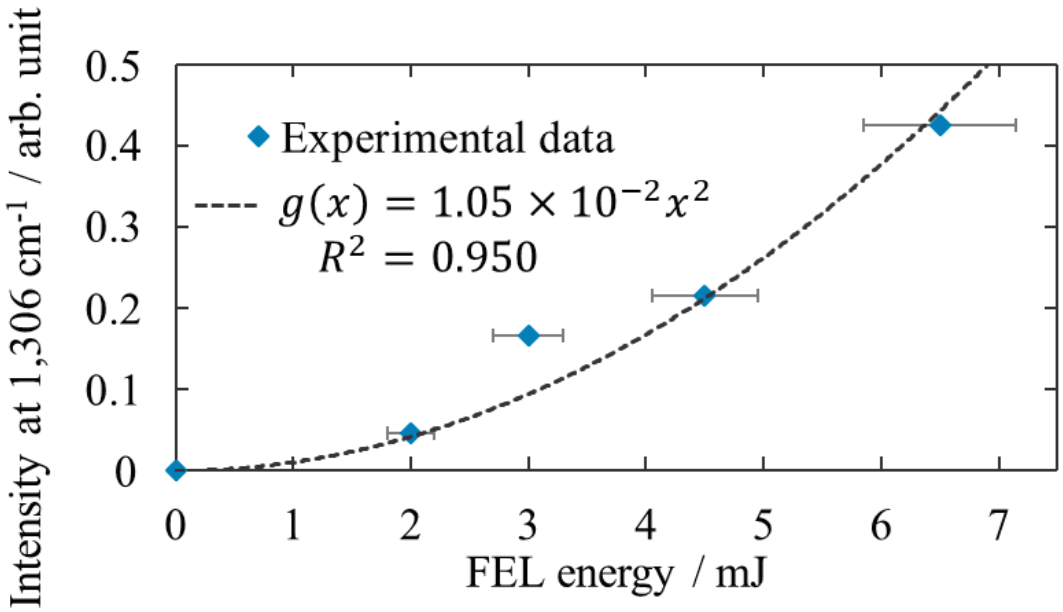

Figure 4: The pump-energy dependence of ASRS peak intensity at $1,306$ cm^{-1} against FEL macropulse energy. A quadratic fitted curve is also given as broken line. The estimation of FEL pulse energy includes an error of about plus or minus 10%.

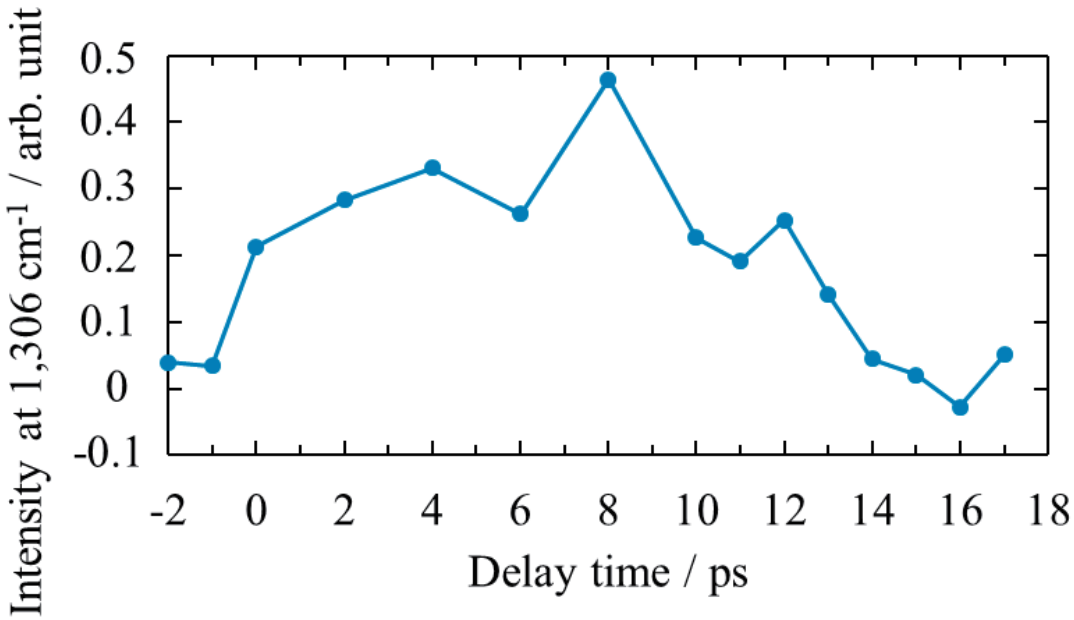

Figure 5: The ASRS peak intensity at $1,306\ \mathrm{cm}^{-1}$ against delay time of probe laser to pump laser.

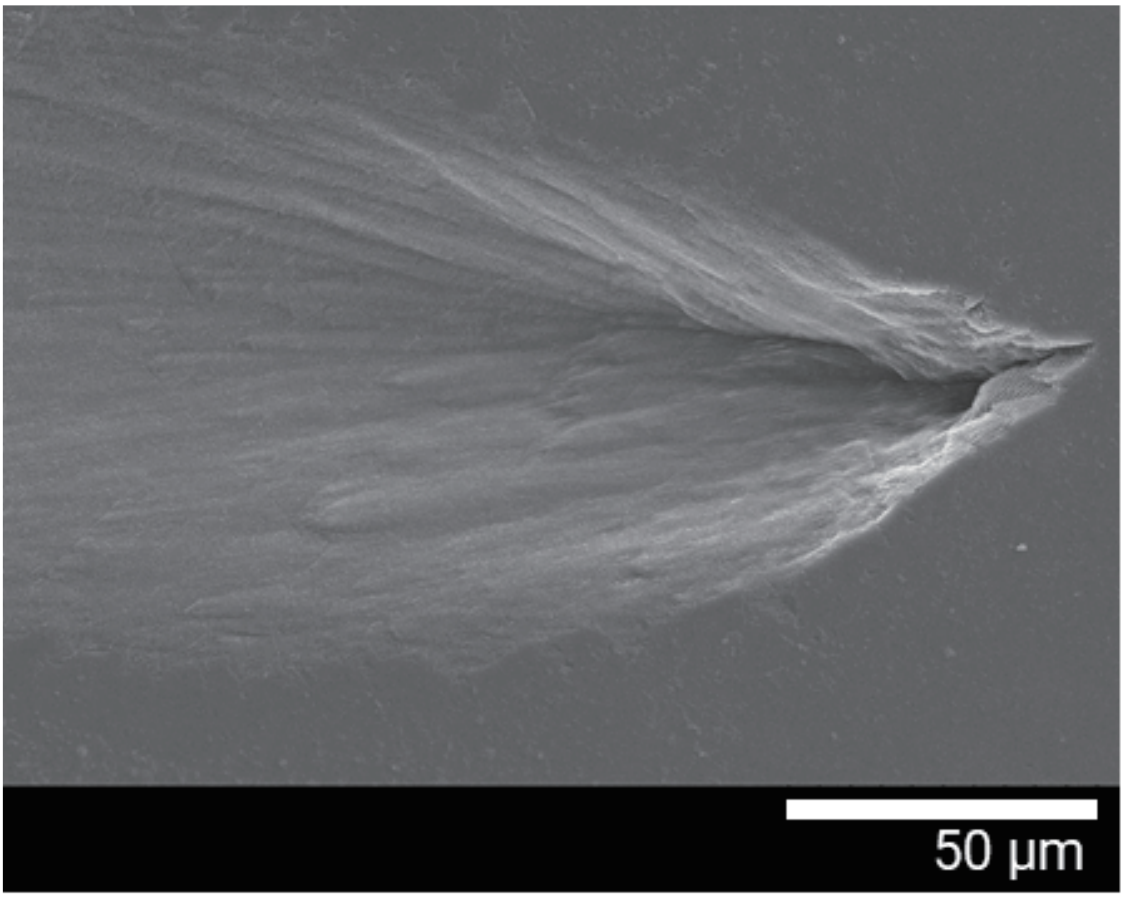

Figure 6: An FE-SEM image of the fracture surface of the damage induced by laser irradiations.